Temperature dependency of the silicon heterojunction lifetime model based on the amphoteric nature of dangling bonds

Vasudevan, R.; Poli, I.; Deligiannis, D.; Zeman, M.; Smets, A.H.M.

DOI
10.1063/1.4968604

Publication date
2016

Document Version
Final published version

Published in
AIP Advances

Temperature dependency of the silicon heterojunction lifetime model based on the amphoteric nature of dangling bonds

R. Vasudevan, I. Poli, D. Deligiannis, M. Zeman, and A. H. M. Smets

Citation: AIP Advances **6**, 115118 (2016); doi: 10.1063/1.4968604
View online: http://dx.doi.org/10.1063/1.4968604
View Table of Contents: http://aip.scitation.org/toc/adv/6/11
Published by the American Institute of Physics

Temperature dependency of the silicon heterojunction lifetime model based on the amphoteric nature of dangling bonds

R. Vasudevan,[a] I. Poli, D. Deligiannis, M. Zeman, and A. H. M. Smets
PVMD, Delft University of Technology, Mekelweg 4, Delft 2628 CD, The Netherlands

(Received 4 July 2016; accepted 11 November 2016; published online 18 November 2016)

This work adapts a model to simulate the carrier injection dependent minority carrier lifetime of crystalline silicon passivated with hydrogenated amorphous silicon at elevated temperatures. Two existing models that respectively calculate the bulk lifetime and surface recombination velocity are used and the full temperature dependency of these models are explored. After a thorough description of these temperature dependencies, experimental results using this model show that the minority carrier lifetime changes upon annealing of silicon heterojunction structures are not universal. Furthermore, comparisons of the temperature dependent model to using the room temperature model at elevated temperatures is given and significant differences are observed when using temperatures above 100 °C. This shows the necessity of taking temperature effects into account during in-situ annealing experiments. [http://dx.doi.org/10.1063/1.4968604]

I. INTRODUCTION

Silicon Heterojunction (SHJ) solar cells are the world record holding silicon-based solar cell technology. Kaneka holds this record with 26.33 % conversion efficiency using the SHJ concept in an interdigitated back contact (IBC) solar cell.[1] In order to improve the performance of solar cells based on this technology a deep understanding of the surface passivation of crystalline silicon (c-Si) wafers using hydrogenated amorphous silicon (a-Si:H) is vital. The passivation quality at the surface is a large factor in achieving the high open circuit voltage (V_{OC}) necessary to reach such high conversion efficiencies.[2] Given the metastable nature of defects in a-Si:H as observed through the Staebler-Wronski Effect,[3] research groups have been investigating the effect of light soaking and annealing on the passivation quality of a-Si:H in SHJ structures.[4,5] One way to investigate this effect is to use photoconductance decay (PCD) measurements to study the carrier injection dependent lifetime of wafers passivated with a-Si:H.[6] In order to extract further information from these measurements, models that link the lifetime measurement to surface defect density (N_S), charge density (Q_S) and capture cross section (σ) can be used.[7,8]

Studies have attempted to understand the nature of c-Si surface passivation by a-Si:H using post-deposition annealing.[5,9] Furthermore, SHJ solar cells have been shown to have very good performance at higher temperatures.[2] Sief et al. has recently linked the performance of SHJ solar cells at high temperatures to lifetime measurements at elevated temperatures of SHJ structures.[10] This study, as well as post-deposition annealing experiments can be run using the lifetime measurement tester with temperature control (WCT-120TS) designed by Sinton Instruments. The complex models used to extract N_S, Q_S and σ from the lifetime measurements contain many parameters that are temperature dependent, though currently the models have only been used at room temperature.[4,5] This manuscript

[a]Electronic mail: r.a.vasudevan@tudelft.nl

first explains, in detail, how these models can be adapted to other temperatures. This is followed by annealing experiments to show a potential application of this temperature dependent model.

II. LIFETIME MODELS USED IN THIS WORK

The foundations for the modeling used in this manuscript are the bulk recombination model of Richter et al. and the surface recombination model that was simplified by Olibet et al.[7,8] Combining these models gives a carrier injection level dependent effective lifetime (τ_{eff}) that can be used to simulate and match the PCD measurements. Using these models, the surface defect density (N_S) and surface charge (Q_S) can be extracted from these PCD measurements (note that there is a charge equivalent in magnitude but opposite in charge to that of Q_S that preserves charge neutrality beneath the surface of the silicon wafer[7]). This is done using the following equation:[11]

$$\frac{1}{\tau_{eff}} = \frac{1}{\tau_{bulk}} + \frac{1}{\tau_{surf}} \tag{1}$$

Where τ_{bulk} is the bulk lifetime and τ_{surf} is the surface lifetime. τ_{surf} can be calculated using the surface recombination velocities by:

$$\frac{1}{\tau_{surf}} = \frac{S_{front}}{W} + \frac{S_{rear}}{W} \tag{2}$$

Where W is the thickness of the silicon wafer, S_{front} is the front surface recombination velocity and S_{rear} is the rear recombination velocity. It should be noted that Equation 2 is a simplification of the relationship between surface recombination velocity and lifetime. This simplification is valid in transient measurements when $S < \frac{D}{4W}$, where S is the surface recombination velocity and D is the diffusion coefficient for silicon.[12,13] For the wafers used in this manuscript (D=11.97 cm^2 s^{-1} and W=280 μm) that means that this simplification works so long as $S < 100$ cm s^{-1}.

In the case that there is a symmetrical structure where S_{front} is equal to S_{rear} this equation can be rewritten equating both surface recombination velocities to an effective surface recombination velocity, S_{eff}.

$$\frac{1}{\tau_{eff}} = \frac{1}{\tau_{bulk}} + \frac{2S_{eff}}{W} \tag{3}$$

In order to extract the desired parameters, N_S and Q_S, τ_{bulk} and S_{eff} must be properly calculated using models for bulk and surface recombination. These models are briefly discussed here to aid the reader in understanding the parameters that are sensitive to temperature.

A. Bulk recombination model

The bulk recombination model used here was proposed by Richter et al.[8] This model calculates radiative and Auger recombination mechanisms for bulk crystalline silicon. Bulk Shockley Read Hall (SRH) recombination is ignored here as the high quality wafers used for SHJ solar cells have defect densities that have a negligible effect on the τ_{eff}. The equation for τ_{bulk} as a function of excess carrier concentration (Δn) is:

$$\tau_{bulk} = \frac{\Delta n}{\left(np - n_i^2\right)\left(2.5\times10^{-31} g_{eeh} n_0 + 8.5\times10^{-32} g_{ehh} p_0 + 3\times10^{-29}\Delta n^{0.92} + B_{rel}B_{low}\right)} \tag{4}$$

Where g_{eeh} and g_{ehh} are enhancement factors introduced by Altermatt et al.:[14]

$$g_{eeh} = 1 + 13\left\{1 - \tanh\left[\left(\frac{n_0}{3.3\times10^{17}}\right)^{0.66}\right]\right\} \tag{5}$$

$$g_{ehh} = 1 + 7.5\left\{1 - \tanh\left[\left(\frac{p_0}{7\times10^{17}}\right)^{0.63}\right]\right\} \tag{6}$$

In Equation 4, B_{low} is the radiative recombination coefficient as measured by Trupke[15] for lightly doped silicon and B_{rel} is the relative radiative recombination coefficient determined by Altermatt.[14] The product of these two coefficients account for the radiative recombination component of bulk crystalline silicon. Both B_{low} and B_{rel} are temperature sensitive. n_i is the intrinsic carrier concentration of silicon, and n_0 and p_0 are the thermal equilibrium concentrations of electrons and holes respectively.

B. Surface recombination velocity model

Once τ_{bulk} has been calculated, the next step is to calculate the surface lifetime (τ_{surf}) which depends on the effective surface recombination velocity (S_{eff}) and the wafer thickness (W). S_{eff} can be calculated by considering the amphoteric nature of dangling bonds in a-Si:H and the c-Si surface.[7] This starts by defining the S_{eff}:

$$S_{eff} \equiv \frac{U_S}{\Delta n} \tag{7}$$

Where U_S is the surface recombination rate. It should be noted here that the Δn used here should actually be the excess carrier concentration of holes (Δp) at the surface of the wafer, since holes are the minority carriers for n-type wafers. In the bulk of the wafer $\Delta p = \Delta n$, but due to the band bending caused by field-effect passivation, this is not the case at the wafer surface. However, Olibet has adapted this calculation and uses the average Δn throughout the bulk of the wafer in place of the Δp at the surface as this value would be too difficult to accurately calculate.[7] This same simplification is used in this manuscript, and Δn is used.

U_S is related to the surface electron and hole densities by:

$$U_S = \frac{n_S \sigma_n^0 \nu_{th\text{-}e} + p_S \sigma_p^0 \nu_{th\text{-}h}}{1 + \frac{p_S \sigma_p^0}{n_S \sigma_n^+} + \frac{n_S \sigma_n^0}{p_S \sigma_p^-}} N_S \tag{8}$$

Where n_S and p_S are the charge carrier surface densities. $\nu_{th\text{-}e}$ and $\nu_{th\text{-}h}$ are the thermal velocities of electrons and holes in silicon and N_S is the surface defect density. σ values here are capture cross sections for defects with designations corresponding to the charge carrier and the direction of carrier capture. These terms are defined as follows:

- σ_n^0 - capture cross section of neutral states for excited electrons
- σ_p^0 - capture cross section of neutral states for holes
- σ_n^+ - capture cross section of positively charged states for excited electrons
- σ_p^- - capture cross section of negatively charged states for holes

A more detailed description of these terms can be found in the work of Olibet et al.[7]

To calculate the n_S and p_S values, the following equations are used:

$$n_S = (n_0 + \Delta n)\, e^{\frac{q(\psi - \phi_n)}{k_B T}} \tag{9}$$

$$p_S = (p_0 + \Delta n)\, e^{\frac{-q(\psi - \phi_p)}{k_B T}} \tag{10}$$

Where n_0 and p_0 are the electron and hole carrier densities at thermal equilibrium, q is the elementary charge, k_B is Boltzmann's constant and T the temperature of the substrate. ϕ_n and ϕ_p are the quasi Fermi levels of electrons and holes at the edge of the space charge region. ψ is the surface potential. Using these parameters, the surface charge can be calculated:

$$Q_S = \pm\sqrt{\frac{2 k_B T n_i \epsilon_0 \epsilon_{Si}}{q^2}\left[e^{\frac{q(\phi_p - \psi)}{k_B T}} - e^{\frac{q\phi_p}{k_B T}} + e^{\frac{q(\psi - \phi_n)}{k_B T}} - e^{\frac{-q\phi_n}{k_B T}} + \frac{q\psi\,(p_0 - n_0)}{k_B T n_i}\right]} \tag{11}$$

Where ϵ_0 is the vacuum permittivity and ϵ_{Si} is the relative permittivity of silicon. Using an iterative fitting method, the n_S and p_S values can be calculated back from a given Q_S value. This eventually can work back to a S_{eff} value that can be used, in combination with τ_{bulk} that was calculated in Equation 4, to fit to a measured τ_{eff} from a PCD measurement. Therefore, Q_S, N_S and σ values can be calculated back from a τ_{eff} measurement. Though this model is a powerful tool to gain information about the passivation quality of a given SHJ sample, care must be taken to ensure its accuracy when the sample is at a temperature above room temperature.

III. TEMPERATURE DEPENDENCIES

In order to perform in-situ annealing experiments using this model, the effects of temperature must first be decoupled from the model. If the goal is to see how N_S, Q_S and the σ values change upon

annealing, one must be very careful to first make sure that all parameters of the model are modified to their proper value at elevated temperature. Seif et al. briefly explained this when exploring the temperature coefficient of silicon heterojunction solar cells.[10] However, this section expands on all of the parameters that have to be accounted for in the model. These are, primarily, the bandgap, effective density of states, the carrier densities, thermal velocity, permittivity and Fermi level. In addition to these semiconductor properties, aspects of recombination processes need to be taken into account, namely, radiative recombination coefficients and σ.

Section III is composed of different parameters used in the model and their temperature dependence. Sources for the temperature dependence of each parameter is given along with how that parameter fits into the overall model for τ_{eff}. Following these descriptions, Section III E illustrates how τ_{eff} changes with temperature once all parameters are taken into account.

A. Carrier concentration

The intrinsic carrier concentration, n_{i} is dependent on the both the bandgap of the material as well as temperature:[16]

$$n_{\text{i}} = n_{\text{i}}(300\text{K})\left(\frac{T}{300}\right)^3 e^{\frac{E_{\text{G}}(T)}{k}\left(\frac{1}{300}-\frac{1}{T}\right)} \tag{12}$$

where n_{i} is linked to the carrier densities n and p by $n_{\text{i}} = \sqrt{np}$. As is noted in Equation 12, the bandgap (E_{G}) also changes with temperature. This has been parametrized by Varshni with the following equation[17]

$$E_{\text{G}}(T) = E_{\text{G}}(0\text{K}) - \frac{\alpha T^2}{T+\beta} \tag{13}$$

Where $E_{\text{G}}(0\text{K})$ of silicon is reported to be 1.170 eV. α and β are material specific constants that were determined to be 4.734×10^{-4} eV/K and 636 K respectively.[18]

In addition to n_{i} the carrier densities at thermal equilibrium n_0 and p_0 need to be calculated as well. For n-type semiconductors this is expressed as:

$$n_0 = \frac{N_{\text{D}}}{2} + \sqrt{\frac{N_{\text{D}}^2}{4} + n_{\text{i}}^2} \tag{14}$$

$$p_0 = \frac{n_{\text{i}}^2}{n_0} \tag{15}$$

Where N_{D} is the donor concentration. In the case of n-type semiconductors, n_0 can be approximated to N_{D}. Though N_{D} can vary at temperatures close to absolute 0, in the temperature range concerning annealing temperatures for SHJ interfaces, N_{D} can be held constant. However, since n_{i} does vary in these temperatures, p_0 has to be adjusted according to the temperature dependent n_{i}. These equations can essentially be duplicated for p-doped silicon with the adjustment that p_0 would remain constant (roughly equal to the acceptor concentration due to doping, N_{A}) while n_0 has to be adjusted for the changing n_{i} values.

B. Thermal velocity

The thermal velocities of holes and electrons ($\nu_{\text{th-h}}$ and $\nu_{\text{th-e}}$) are needed to calculate the recombination rate in Equation 8. These values are dependent on temperature:[16]

$$\nu_{\text{th-h}} = \sqrt{\frac{8k_{\text{B}}T}{\pi m_{\text{h}}}} \tag{16}$$

$$\nu_{\text{th-e}} = \sqrt{\frac{8k_{\text{B}}T}{\pi m_{\text{e}}}} \tag{17}$$

Where m_{h} is the effective mass of holes (7.29×10^{-31} kg) and m_{e} is the effective mass of electrons (5.10×10^{-31} kg).

C. Fermi level

Equation 11 is also dependent on the Fermi level of silicon. The Fermi level, however, is also dependent on temperature with the relationship for n-type:[11]

$$E_F - E_{Fi} = k_B T \ln\left(\frac{n_0}{n_i}\right) \tag{18}$$

and the relationship for p-type:

$$E_F - E_{Fi} = -k_B T \ln\left(\frac{p_0}{n_i}\right) \tag{19}$$

Where E_{Fi} is the intrinsic Fermi level, which is assumed here to be the middle of the bandgap.

D. Bulk recombination properties

Equation 4 shows the model used for calculating τ_{bulk}. The two radiative coefficients B_{rel} and B_{low} are temperature dependent. The temperature dependence of the product of B_{rel} and B_{low} (B) has been demonstrated by Altermatt and that relationship is used here.[14,19]

E. Model outcomes

The temperature dependencies of the lifetime models are shown in FIG 1. For these calculations a sample thickness of 280 μm was used. An N_S of 1×10^9 cm^{-2} and a Q_S of -1×10^9 cm^{-2} were used. The capture cross section ratios were: $\frac{\sigma_n^0}{\sigma_p^0} = 0.2$ and $\frac{\sigma_p^-}{\sigma_p^0} = \frac{\sigma_n^+}{\sigma_n^0} = 500$. These values were all held constant, while the temperature dependencies described in the previous section were considered. Therefore this figure shows how a change in temperature affects the different lifetime values, even if no annealing is taking place.

FIG 1a shows how τ_{bulk} varies with temperature according to the parameters described above. Note that there is practically no difference between the τ_{bulk} curves as a function of temperature. However, FIG 1b shows that S_{eff} does, indeed, change with temperature. Finally, FIG 1c shows the changes in the final τ_{eff} parameter as a function of temperature. It is clear here that in the injection levels of interest, there are significant changes in lifetime due to temperature. Overall, τ_{eff} decreases with temperature. If the temperature dependencies discussed in this chapter are not properly accounted

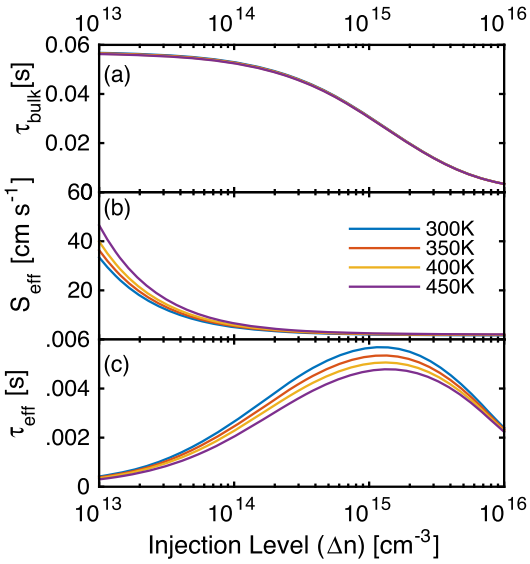

FIG. 1. Model variations based on temperature. (a) shows the bulk lifetime τ_{bulk} as a function of carrier injection over a variety of temperatures with no practical variation, (b) shows the effective surface recombination velocity (S_{eff}) as a function of carrier injection level over a variety of temperatures and (c) shows the final effective lifetime τ_{eff} as a function of carrier injection level under the same variety of temperatures.

for, differences in lifetime may be attributed to annealing when these differences are simply the result of property changes at elevated temperatures.

IV. EXPERIMENTAL RESULTS

In-situ annealing experiments were carried out on three passivated samples. The goal of these experiments was to examine c-Si wafers passivated with a-Si:H to gather insights into the annealing kinetics of the a-Si:H/c-Si heterojunction interface. The results of the experiments and the model outcomes are given first. This is followed by a comparison of the fitting results using the temperature adjusted model to the fitting results using the model at room temperature.

A. Experimental details

Float zone, double polished, n-type c-Si wafers with ⟨111⟩ crystal orientation are used. These wafers have a diameter of 4 inches and a thickness of 280 μm. The resistivity of the wafers is between 2 Ω cm to 5 Ω cm Wafers were cleaned using a three step wet chemical cleaning procedure described elsewhere.[20] Both sides of each wafer were symmetrically passivated with 30 nm of a-Si:H using plasma enhanced chemical vapor deposition (PECVD). The thickness of a-Si:H was held constant in order to account for thickness dependent effects on the lifetime.[21] Two different sets of deposition conditions for the a-Si:H were used. The first method, referred to here as undiluted a-Si:H was prepared using 40 sccm of SiH_4 at 0.7 mbar and at a power density of 0.015 W cm^{-2}. The second method, referred to here as diluted a-Si:H, was deposited using 4 sccm SiH_4 and 200 sccm H_2 at 8 mbar and at a power density of 0.056 W cm^{-2}. This second method has been shown to have good properties for both passivation and use in thin-film solar cells.[22,23] Both methods deposited at a substrate temperature of 180 °C and stay in the amorphous regime of thin-film silicon.

After the samples were prepared they were moved to the Sinton WCT 120-TS for τ_{eff} measurements. The stage has a controllable temperature. Samples were placed on the stage at room temperature and then the τ_{eff} was monitored at regular temperature increments until the stage reached 150 °C. At this point the temperature stage remained at 150 °C for two hours while the samples were measured at regular temperature intervals to monitor changes in the passivation quality during annealing. Each lifetime measurement both in the temperature ramp up phase and the longer term annealing phase represents an average of five measurements. Error bars on the fitting results represent the confidence interval of that parameter in the fit.

B. Annealing experiments using the temperature adjusted model

FIG 2 shows the results of the annealing experiment run on a sample using undiluted a-Si:H. In this case it is observed that the Q_S value stays within error margins throughout the annealing process while the N_S decreases as the sample is annealed. This is consistent with the findings of De Wolf et al.[9] However, this is not always the case. FIG 3 shows a repetition of this experiment. here a new sample was produced with identical deposition conditions, however, the N_S value stays within fitting error throughout the temperature ramp-up and extended annealing. Though it is unclear exactly why this sample exhibited a lower susceptibility to annealing induced reduction of N_S, this shows that samples passivated with a-Si:H do not always exhibit increased passivation quality upon thermal annealing.

Another finding from FIG 3 is that though τ_{eff} curves, indeed, change significantly throughout the changes in temperature as shown in FIG 3a, the model does not show a corresponding change in N_S when differences in temperature are taken into account in FIG 3c. This shows importance of using this model when characterizing in-situ annealing experiments for c-Si wafers passivated with a-Si:H as changes in τ_{eff} may be due only to the material properties of Si changing due to elevated temperatures rather than an actual reduction of N_S.

FIG 4 shows the results of the annealing experiment run on a sample using diluted a-Si:H. This method of a-Si:H passivation has been shown to be very susceptible to annealing effects especially when deposited at lower temperatures.[22,23] Using this in-situ experimental method, it is revealed

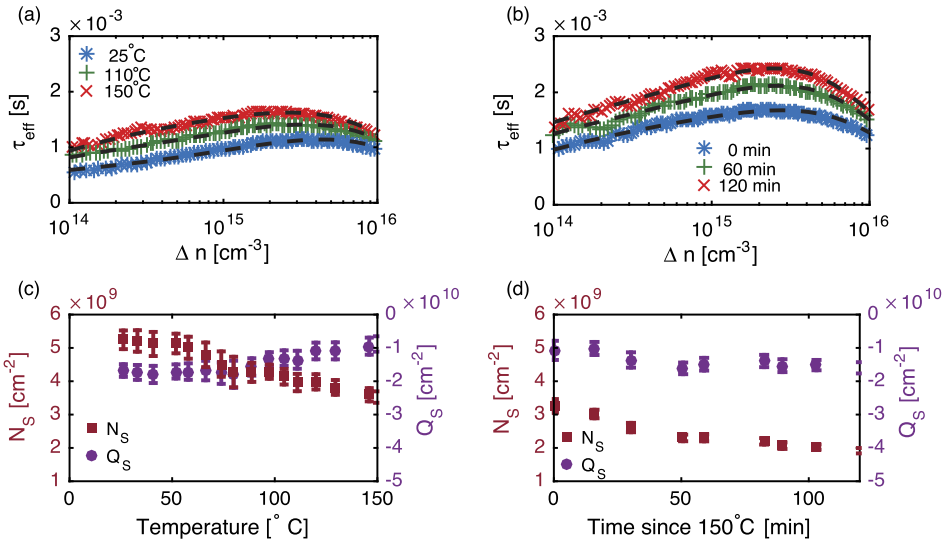

FIG. 2. Annealing experiment on a c-Si wafer passivated with undiluted a-Si:H. (a) Carrier injection dependent lifetime of the sample at three different temperatures. Black dashed lines represent the model that was fit to the measurements, which are represented by colored markers. (b) Carrier injection dependent lifetime of the sample at three different annealing times once temperature has stabilized to 150 °C. Black dashed lines represent the model that was fit to the measurements, which are represented by colored markers. (c) Fitting results of parameters N_S (left axis) and Q_S (right axis) at different temperatures. (d) Fitting results of parameters N_S (left axis) and Q_S (right axis) at different annealing times.

that most of the improvements in diluted a-Si:H passivation occur on very fast timescales during the temperature ramp up, itself. FIG 4c in particular shows that the majority of the reduction of N_S occurs during the temperature ramp-up from around 70 °C to 150 °C, while a small decrease in N_S is apparent during the two hour annealing process.

These results illustrate the potential of using the temperature model given in Section III in conjunction with annealing experiments. The model helps to distinguish between changes in

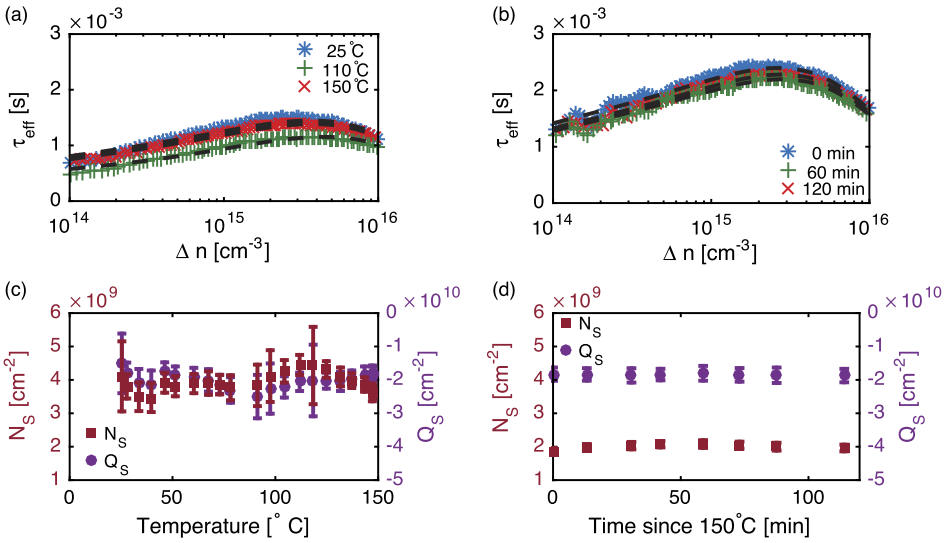

FIG. 3. Repetition of annealing experiment on a c-Si wafer passivated with undiluted a-Si:H as shown in FIG 2. (a) Carrier injection dependent lifetime of the sample at three different temperatures. Black dashed lines represent the model that was fit to the measurements, which are represented by colored markers. (b) Carrier injection dependent lifetime of the sample at three different annealing times once temperature has stabilized to 150 °C. Black dashed lines represent the model that was fit to the measurements, which are represented by colored markers. (c) Fitting results of parameters N_S (left axis) and Q_S (right axis) at different temperatures. (d) Fitting results of parameters N_S (left axis) and Q_S (right axis) at different annealing times.

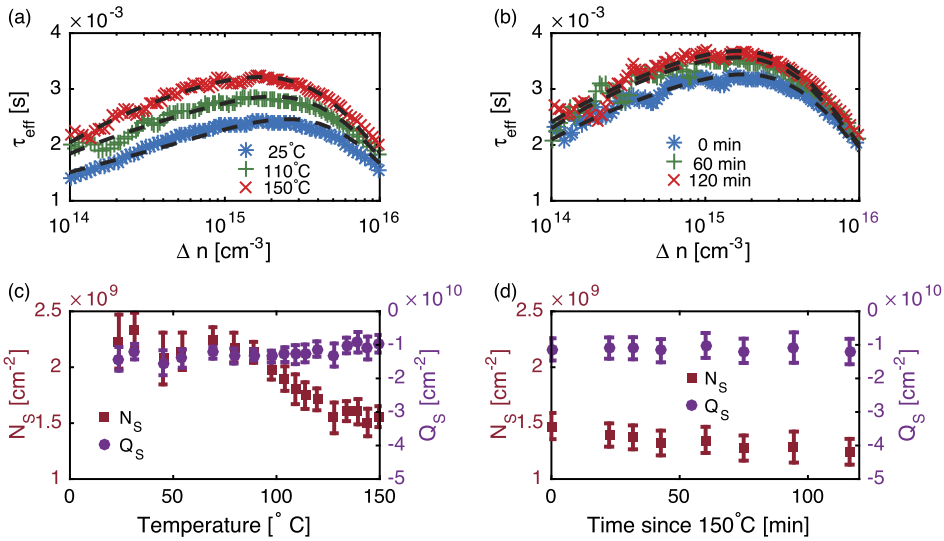

FIG. 4. Annealing experiment on a c-Si wafer passivated with diluted a-Si:H. (a) Carrier injection dependent lifetime of the sample at three different temperatures. Black dashed lines represent the model that was fit to the measurements, which are represented by colored markers. (b) Carrier injection dependent lifetime of the sample at three different annealing times once temperature has stabilized to 150 °C. Black dashed lines represent the model that was fit to the measurements, which are represented by colored markers. (c) Fitting results of parameters N_S (left axis) and Q_S (right axis) at different temperatures. (d) Fitting results of parameters N_S (left axis) and Q_S (right axis) at different annealing times.

τ_{eff} that are due to changes in passivation quality and charge buildup from changes in τ_{eff} that are due to changes in the properties of Si at elevated temperatures. The results from the experiments presented in FIG 2, 3 and 4 show that τ_{eff} kinetics of a-Si:H passivated samples are not universal. Further experimentation using this model can help to better understand the nature of these annealing kinetics and any potential effects it has on silicon heterojunction solar cell performance.

C. Comparison of temperature dependent model to room temperature model

To illustrate the utility of the temperature dependent model described in this manuscript, a comparison was done on the three experiments outlined above. FIG 5 shows how the outputs of the model (N_S and Q_S) vary when using the temperature dependent model and when temperature is ignored.

FIG 5a shows that in both the diluted a-Si:H and the undiluted a-Si:H, the τ_{eff} model is significantly temperature dependent when trying to calculate N_S from the τ_{eff} at temperatures above 100 °C as calculations of N_S from either model are outside of the error margin of the calculation of the other model. This continues with the annealing experiment at 150 °C in FIG 5b. In contrast, Figures 5c and d show that Q_S stays within the error margins when fitting using either the temperature dependent model or the room temperature model.

The differences in N_S are more pronounced at higher defect densities. This is shown in Figures 5a and b when comparing the undiluted case (higher N_S) to the diluted case. In the undiluted case, there is a larger difference between using the temperature dependent model and the room temperature model. Looking closer at the results in FIG 5b also confirms this. As the N_S value reduces due to annealing, the calculated values of the models get closer together and thus the effect of temperature becomes negligible.

These results suggest that if calculating N_S from a τ_{eff} measurement is the primary objective then it is useful to use this temperature correction if the sample is elevated to over 100 °C. However, if Q_S is all that is needed, using the temperature correction here will not yield a significant difference.

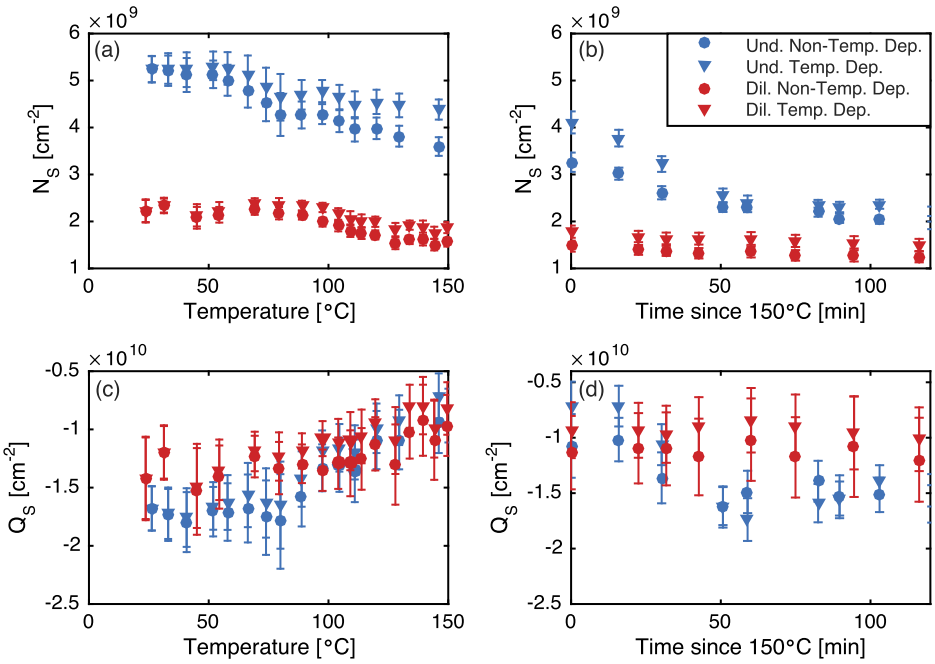

FIG. 5. Comparison of temperature dependent model to using the room temperature model. In all figures the blue markers correspond to fittings done on data from FIG 2 (undiluted a-Si:H) and red markers correspond to fittings done on data from FIG 4 (diluted a-Si:H). Triangles correspond to fittings done using the temperature dependent model and circles correspond to fittings using the standard room temperature model. (a) Defect density vs Temperature during the temperature ramp up from room temperature to 150 °C. (b) Defect density vs annealing time at 150 °C. (c) Charge density vs Temperature during the temperature ramp up from room temperature to 150 °C. (d) Charge density vs annealing time at 150 °C.

V. CONCLUSIONS

This manuscript has shown how the models of Richter[8] and Olibet[7] can be modified in order to account for temperature to calculate back the passivation quality from measured τ_{eff} values. Properties of Si such as the carrier concentration, thermal velocity and Fermi level are all temperature dependent and these values affect the calculation of τ_{eff} as a function of N_S, Q_S and σ ratios. The effect of temperature on the calculation given constant passivation quality values has been demonstrated. Furthermore sample in-situ annealing experiments have been carried out to show that different types of a-Si:H can exhibit different annealing kinetics that are only apparent by using a temperature dependent lifetime model. Finally a comparison of using the temperature dependent model and the room temperature model given in literature has been carried out. This shows that correcting for temperature is significant when calculating N_S over 100 °C, but not significant when calculating Q_S up to 150 °C. This tool can now be used in further experimentation to better understand the nature of annealing induced improvements in passivation quality of c-Si by a-Si:H.

ACKNOWLEDGMENTS

The authors of this paper would like to acknowledge the Martijn Tijssen, Stefan Heirman and Remko Koornneef for their invaluable technical assistance on all aspects of this project. This project was done through the funding of STW in the Fundamentals of Silicon Heterojunctions (FLASH) consortium in the Netherlands under the grant number 12166.

[1] Kaneka, "World 's Highest Conversion Efficiency of 26.33% Achieved in a Crystalline Silicon Solar Cell - A World First in a Practical Cell Size -," Press Release (2016).
[2] S. De Wolf, A. Descoeudres, Z. C. Holman, and C. Ballif, "High-efficiency silicon heterojunction solar cells: A review," Green **2**, 7–24 (2012).
[3] D. L. Staebler and C. R. Wronski, "Reversible conductivity changes in discharge-produced amorphous Si," Applied Physics Letters **31**, 292 (1977).

[4] S. De Wolf, B. Demaurex, A. Descoeudres, and C. Ballif, "Very fast light-induced degradation of a-Si:H/c-Si(100) interfaces," Physical Review B **83**, 233301 (2011).
[5] P. Mahtani, R. Varache, B. Jovet, C. Longeaud, J.-P. Kleider, and N. P. Kherani, "Light induced changes in the amorphous/crystalline silicon heterointerface,"Journal of Applied Physics **114**, 124503 (2013).
[6] R. A. Sinton, "Quasi-steady-state photoconductance, a new method for cell material and device characterization," in 25th PVSC (1996) pp. 457–460.
[7] S. Olibet, E. Vallat-Sauvain, and C. Ballif, "Model for a-Si:H/c-Si interface recombination based on the amphoteric nature of silicon dangling bonds," Physical Review B **76**, 035326 (2007).
[8] A. Richter, S. W. Glunz, F. Werner, J. Schmidt, and A. Cuevas, "Improved quantitative description of Auger recombination in crystalline silicon," Physical Review B **86**, 165202 (2012).
[9] S. De Wolf, S. Olibet, and C. Ballif, "Stretched-exponential a-Si:Hc-Si interface recombination decay," Applied Physics Letters **93**, 032101 (2008).
[10] J. P. Seif, G. Krishnamani, C. Ballif, and S. D. Wolf, "Amorphous/crystalline silicon interface passivation: Ambient-temperature dependence and implications for solar cell performance," IEEE Journal of Photovoltaics **5**, 718–724 (2015).
[11] S. Rein, in *Lifetime Spectroscopy: A Method of Defect Characterization in Silicon for Photovoltaic Applications*, edited by R. Hull, J. Parisi, R. M. Osgood, and H. Warlimont (Verlag Berlin Heidelberg, 2006).
[12] J. Brody, A. Rohatgi, and A. Ristow, "Review and comparison of equations relating bulk lifetime and surface recombination velocity to effective lifetime measured under flash lamp illumination," Solar energy materials and solar cells **77**, 293–301 (2003).
[13] A. B. Sproul, "Dimensionless solution of the equation describing the effect of surface recombination on carrier decay in semiconductors," Journal of Applied Physics **76**, 2851 (1994).
[14] P. P. Altermatt, F. Geelhaar, T. Trupke, X. Dai, A. Neisser, and E. Daub, "Injection dependence of spontaneous radiative recombination in c-Si: Experiment, theoretical analysis, and simulation," *NUSOD '05-Proceedings of the 5th International Conference on Numerical Simulation of Optoelectronic Devices 2005*, 47–48 (2005).
[15] T. Trupke, M. A. Green, P. Würfel, P. P. Altermatt, A. Wang, J. Zhao, and R. Corkish, "Temperature dependence of the radiative recombination coefficient of intrinsic crystalline silicon," Journal of Applied Physics **94**, 4930–4937 (2003).
[16] R. F. Pierret, New York (1996) p. 792.
[17] Y. Varshni, "Temperature dependence of the energy gap in semiconductors," Physica **34**, 149–154 (1967).
[18] D. Wolpert and P. Ampadu, *Managing Temperature Effects in Nanoscale Adaptive Systems* (2012), pp. 15–34.
[19] P. P. Altermatt, F. Geelhaar, T. Trupke, X. Dai, A. Neisser, and E. Daub, "Injection dependence of spontaneous radiative recombination in crystalline silicon: Experimental verification and theoretical analysis," Applied Physics Letters **88**, 92–95 (2006).
[20] D. Zhang, I. Digdaya, R. Santbergen, R. van Swaaij, P. Bronsveld, M. Zeman, J. van Roosmalen, and A. Weeber, "Design and fabrication of a SiOx/ITO double-layer anti-reflective coating for heterojunction silicon solar cells," Solar Energy Materials and Solar Cells **117**, 132–138 (2013).
[21] D. Deligiannis, V. Marioleas, R. Vasudevan, C. C. G. Visser, R. A. C. M. M. van Swaaij, and M. Zeman, "Understanding the thickness-dependent effective lifetime of crystalline silicon passivated with a thin layer of intrinsic hydrogenated amorphous silicon using a nanometer-accurate wet-etching method," Journal of Applied Physics **119**, 235307 (2016).
[22] M. Fischer, H. Tan, J. Melskens, R. Vasudevan, M. Zeman, and A. H. M. Smets, "High pressure processing of hydrogenated amorphous silicon solar cells: Relation between nanostructure and high open-circuit voltage," Applied Physics Letters **106**, 043905 (2015).
[23] D. Deligiannis, R. Vasudevan, A. H. M. Smets, R. A. C. M. M. V. Swaaij, and M. Zeman, "Surface passivation of c-Si for silicon heterojunction solar cells using high-pressure hydrogen diluted plasmas," AIP Advances **5**, 097165 (2015).